



CHORUS

This is the accepted manuscript made available via CHORUS. The article has been published as:

Asymptotic normalization coefficients and spectroscopic factors from deuteron stripping reactions

D. Y. Pang and A. M. Mukhamedzhanov

Phys. Rev. C **90**, 044611 — Published 21 October 2014

DOI: [10.1103/PhysRevC.90.044611](https://doi.org/10.1103/PhysRevC.90.044611)

Asymptotic normalization coefficients and spectroscopic factors from deuteron stripping reactions

D. Y. Pang

School of Physics and Nuclear Energy Engineering,

Beihang University, Beijing 100191, China,

Cyclotron Institute, Texas A&M University, College Station, TX 77843, USA

A. M. Mukhamedzhanov

Cyclotron Institute, Texas A&M University, College Station, TX 77843, USA

(Dated: Today)

Abstract

We present the analysis of three deuteron stripping reactions, $^{14}\text{C}(d,p)^{15}\text{C}$, $^{58}\text{Ni}(d,p)^{59}\text{Ni}$ and $^{116}\text{Sn}(d,p)^{117}\text{Sn}$ using the combined method [A. M. Mukhamedzhanov and F. M. Nunes Phys. Rev. **C 72**, 017602 (2005)], in which each reaction is analyzed at low and significantly higher energies. At low energies all these reactions are peripheral and the experimental asymptotic normalization coefficients (ANCs) are determined with accuracy about 10%. At higher energies we determine the spectroscopic factors (SFs) by fixing the normalization of the peripheral parts of the reaction amplitudes governed by the ANCs found from the low-energy data. The combined method imposes a strict limitation on the variation of the geometrical parameters of the single-particle potential, which can be arbitrarily taken in the standard approach. By checking the compatibility of the ANCs and SFs using the combined method we reveal the flaw in the contemporary nuclear reaction theory in treating the nuclear interior, which is the most crucial part in the determination of the SFs.

PACS numbers: 25.45.-z, 24.50.+g, 21.10.Jx, 24.10.Eq

I. INTRODUCTION

One of the main purposes of measuring transfer reactions is to extract spectroscopic information important for nuclear structure, nuclear astrophysics and applied physics. Deuteron stripping reactions pioneered the usage of the transfer reactions being the simplest transfer reactions, which still carry many features of reactions with composite nuclei. For more than 50 years deuteron stripping reactions were one of the main tools to determine spectroscopic factors (SFs) and later on, asymptotic normalization coefficients (ANCs). Determination of these important quantities is based on measuring the overlap function of the bound state wave functions of the final and initial nuclei in the deuteron stripping reactions. Changing the reaction kinematics, energy, and target one can probe different parts of the overlap function.

At low energies and good matching of the initial and final momenta the reaction is dominantly peripheral, that is, the reaction amplitude is mainly contributed by the peripheral part of the overlap function. In this case normalization of the theoretical differential cross section to the experimental one allows us to determine the ANC. That is why we can say that the ANC controls the overall normalization of the peripheral deuteron stripping reactions. With the energy and/or mismatching of the initial and final momenta increase the contribution of the nuclear interior also increases allowing one to determine the SF. However, the external part still contributes significantly. To extract the SF with better precision in [1, 2] the normalization of the external part was fixed using experimentally measured ANC from a different peripheral reaction. Such a combined method allows one not only to extract the SF with a better accuracy but also to test an underlying nuclear reaction theory.

Such an analysis has been done in [2–5] using distorted wave Born approximation (DWBA) and adiabatic distorted wave approximation (ADWA). The latest analysis has been done in [5], where the $^{14}\text{C}(d, p)^{15}\text{C}$ reaction at the deuteron energy $E_d = 23.4$ and 60 MeV was analyzed. Because the low-energy reaction is peripheral, the ANC for the neutron removal from ^{15}C was determined from its analysis and then the combined method was applied to determine the SF from the higher energy deuteron stripping reaction. Introduction into the analysis the ANC by fixing the normalization of the external part of the reaction amplitude leads to unrealistical SFs for the ground and the first excited states of ^{15}C . In the combined method the reliability of the extracted SF depends on the accuracy

of the reaction theory in the calculation of the internal part of the reaction amplitude. The failure to determine reliable SF in [5] can be caused by two reasons: the inaccuracy of the adopted ADWA reaction theory, and ambiguity in the adopted optical potentials. The used Koning-Delaroche (KD) potential [6] and CH89 [7] are not determined for light nuclei as $^{14,15}\text{C}$. The impact of the optical potentials was demonstrated by the dependence of the results on the adopted optical potentials.

Because the combined method can reveal shortcomings of the underlying reaction theory and indicate directions in which it can be improved we apply a more deeper and updated analysis of three different deuteron stripping reactions on light, medium and heavier nuclei, $^{14}\text{C}(d, p)^{15}\text{C}$, $^{58}\text{Ni}(d, p)^{59}\text{Ni}$ and $^{116}\text{Sn}(d, p)^{117}\text{Sn}$. In all three cases the final neutron bound state wave functions have nodes. While the neutron bound state in ^{15}C is loosely bound, the two other nuclei have tightly bound neutrons.

To check the dependence of the extracted ANCs and SFs on the reaction model we compared the results of the DWBA, ADWA and continuum discretized coupled-channels (CDCC) for these reactions at two different energies. First we analyze each reaction at low energy, where each reaction is peripheral and we are able to determine the ANC. After that to apply the combined method we analyze all three reactions at higher energies, where reactions are not peripheral and internal parts of the reaction amplitude become more significant. Since the SF is mainly contributed by the nuclear interior from the analysis of the reactions at higher energies we can determine the SF at fixed normalization of the peripheral part of the reaction amplitude using the information about the ANC obtained from the analysis of the low-energy data. The extracted SFs are compared with the ones obtained using the standard analysis followed by the critical analysis of the theory. Note that in the analysis of the $^{14}\text{C}(d, p)^{15}\text{C}$ reaction we added the CDCC method, which was absent in [5]. Two other reactions were selected because for heavier nuclei the KD optical potentials [6] and CH89 [7] potentials are available making results of the analysis more reliable, so that the combined method of determination of the SF, which uses the information about the ANC, can be tested more accurately.

II. REACTION MODELS

In the analysis we used three reaction models, DWBA, ADWA and CDCC. The deuteron stripping amplitude can be written in the post form:

$$M^{TH(post)} = \langle \chi_{pF}^{(-)} I_A^F | \Delta V_{pF} | \Phi_i^{(+)} \rangle, \quad (1)$$

where the acronym TH stands for the DWBA, ADWA or CDCC. In the DWBA the initial channel wave function $\Phi_i^{(+)}$ is given by

$$\Phi_i^{(+)} = \varphi_{pn} \chi_{dA}^{(+)}. \quad (2)$$

For the ADWA we use the same channel wave function as in the DWBA but the $d - A$ optical potential generating the initial distorted wave is taken as prescribed in the Johnson-Tandy model [8]. In the CDCC approach we replace $\Phi_i^{(+)}$ by the CDCC wave function, which is given by the sum of the incident channel wave function $\varphi_d \chi_{dA}^{(+)}$ and the three-body continuum state $p + n + A$. In the three-body continuum the integration over the $n - A$ relative momentum k_{nA} is replaced by the summation over the bins [9]. The final channel wave function is taken in the same form as in the DWBA. φ_{pn} is the deuteron bound state wave function, $\chi_{ij}^{(\pm)}$ is the distorted wave of particles i and j interacting via the optical potential U_{ij} , $I_A^F = \sqrt{A+1} \langle \varphi_A | \varphi_F \rangle$ is the overlap function of the bound state wave functions of nuclei $F = (n A)$ and A , $\sqrt{A+1}$ is the antisymmetrization factor in the isospin formalism.

$$\Delta V_{pF} = U_{pA} + V_{pn} - U_{pF}, \quad (3)$$

where V_{pn} is the $p - n$ interaction potential. We use KD optical potentials as the $N - A$ optical ones for the analysis of the reactions on ^{14}C and ^{58}Ni . For the analysis of the reactions on ^{116}Sn we use the CH89 $N - A$ optical potentials. In the DWBA the distorted wave $\chi_{dA}^{(+)}$ is calculated using a global optical potential. In the ADWA the optical potential U_{dA} is expressed in terms of the proton and neutron optical potentials [8].

III. COMBINED METHOD OF DETERMINATION OF SPECTROSCOPIC FACTOR

The overlap function appearing in the DWBA, ADWA and CDCC is not an eigenfunction of an Hermitian Hamiltonian and is not normalized to unity [10]. The square norm of the

overlap function gives a model-independent definition of the SF:

$$S = \sqrt{A + 1} \langle I_A^F | I_A^F \rangle, \quad (4)$$

where the antisymmetrization factor is taken in the isospin formalism. From now on we absorb the antisymmetrization factor into the overlap function.

The tail of the radial overlap function is given by

$$I_{A(l_{nA}j_{nA})}^F(r_{nA}) \stackrel{r_{nA} \gg R_{nA}}{\approx} C_{l_{nA}j_{nA}} i \kappa_{nA} h_{l_{nA}}^{(1)}(i \kappa_{nA} r_{nA}), \quad (5)$$

where $h_{l_{nA}}^{(1)}(i \kappa_{nA} r_{nA})$ is the spherical Hankel function, $\kappa_{nA} = \sqrt{2 \mu_{nA} \varepsilon_{nA}}$, ε_{nA} is the binding energy for $F \rightarrow n + A$, and μ_{nA} is the reduced mass of n and A ; l_{nA} and j_{nA} are the orbital angular momentum and the total angular momentum of the neutron in the bound state $F = (nA)$. Similarly, the asymptotics of the neutron single-particle wave function is

$$\varphi_{nA(n_r l_{nA} j_{nA})}(r_{nA}) \stackrel{r_{nA} \gg R_{nA}}{\approx} b_{n_r l_{nA} j_{nA}} i \kappa_{nA} h_{l_{nA}}^{(1)}(i \kappa_{nA} r_{nA}), \quad (6)$$

where $b_{n_r l_{nA} j_{nA}}$ is the single-particle ANC (SPANC) determining the amplitude of the tail of the single-particle bound state wave function and n_r is the principle quantum number. The asymptotic behaviour is valid beyond R_{nA} , the nuclear interaction radius. It is clear that in the asymptotic region the overlap function is proportional to the single particle wave function.

The normalization $C_{l_{nA}j_{nA}}$ introduced in Eq. (5) is the ANC which relates to the SPANC $b_{n_r l_{nA} j_{nA}}$ by $C_{l_{nA}j_{nA}} = K_{n_r l_{nA} j_{nA}} b_{n_r l_{nA} j_{nA}}$, where $K_{n_r l_{nA} j_{nA}}$ is an asymptotic proportionality coefficient. It is a standard practice to assume that the proportionality between the overlap function and the single particle function extends to all r_{nA} values

$$I_{nA(l_{nA}j_{nA})}^F(r_{nA}) = K_{n_r l_{nA} j_{nA}} \varphi_{nA(n_r l_{nA} j_{nA})}(r_{nA}). \quad (7)$$

Since $\varphi_{nA(n_r l_{nA} j_{nA})}(r_{nA})$ is normalized to unity, this approximation, Eq. (7), implies that

$$SF_{n_r l_{nA} j_{nA}} = K_{n_r l_{nA} j_{nA}}^2. \quad (8)$$

Thus, although the definition (4) of the SF does not depend on the principal quantum number n_r , approximation (7) of the overlap function by the single-particle wave function leads to the SF, Eq. (8), which depends on n_r .

We have to emphasize, however, that the behavior of the overlap function in the interior is nontrivial and may well differ from the single particle wave function. Approximating the radial dependence of the overlap function as described above leads to the post form of the stripping amplitude

$$M^{TH(post)} = SF_{n_r l_{nA} j_{nA}}^{1/2} \langle \chi_{pF}^{(-)} \varphi_{nA(n_r l_{nA} j_{nA})} | \Delta V_{pF} | \Phi_i^{(+)} \rangle, \quad (9)$$

Normalizing the calculated cross section,

$$\frac{d\sigma^{TH(post)}}{d\Omega} = | \langle \chi_{pF}^{(-)} \varphi_{nA(n_r l_{nA} j_{nA})} | \Delta V_{pF} | \Phi_i^{(+)} \rangle |^2 \quad (10)$$

to the experimental data provides the phenomenological SF $SF_{n_r l_{nA} j_{nA}} = K_{n_r l_{nA} j_{nA}}^2$. Assuming that Eq. (7) is valid for all r_{nA} , we can infer from Eq. (4) that the main contribution to the norm of the overlap function comes from the nuclear interior (except for very loosely bound neutrons). In the meantime, the normalization amplitude of the asymptotic tail of the overlap function is determined by the ANC. Correspondingly let us rewrite the reaction amplitude in terms of the internal and external (over the variable r_{nA}) parts:

$$M^{TH(post)} = M_{int}^{TH(post)} + M_{ext}^{TH(post)}. \quad (11)$$

Here, the internal matrix element is

$$M_{int}^{TH(post)} = SF_{n_r l_{nA} j_{nA}}^{1/2} \tilde{M}_{int}^{TH(post)}, \quad (12)$$

$$\tilde{M}_{int}^{TH(post)} = \langle \chi_{pF}^{(-)} \varphi_{nA(n_r l_{nA} j_{nA})} | \Delta V_{pF} | \Phi_i^{(+)} \rangle \Big|_{r_{nA} \leq R_{nA}}. \quad (13)$$

Correspondingly, the external matrix element is

$$M_{ext}^{TH(post)} = SF_{n_r l_{nA} j_{nA}}^{1/2} \langle \chi_{pF}^{(-)} \varphi_{nA(n_r l_{nA} j_{nA})} | \Delta V_{pF} | \Phi_i^{(+)} \rangle \Big|_{r_{nA} \geq R_{nA}} \quad (14)$$

Note that the integration in Eqs (13) and (14) over the second Jacobian variable, the radius-vector between the outgoing proton and the center of mass of F ρ_{pF} , is taken over the whole volume.

Taking into account Eq. (6) we can rewrite the external matrix element as

$$M_{ext}^{TH(post)} = C_{l_{nA} j_{nA}} \tilde{M}_{ext}^{TH(post)}, \quad (15)$$

where

$$\tilde{M}_{ext}^{TH(post)} = i \kappa_{n_A} \langle \chi_{pF}^{(-)} h_{l_{n_A}}^{(1)}(i \kappa_{n_A} r_{n_A}) | \Delta V_{pF} | \Phi_i^{(+)} \rangle \Big|_{r_{n_A} \geq R_{n_A}}. \quad (16)$$

The normalization factor in Eq. (15) is nothing else but the ANC

$$C_{l_{n_A} j_{n_A}} = S F_{n_r l_{n_A} j_{n_A}}^{1/2} b_{n_r l_{n_A} j_{n_A}}. \quad (17)$$

Note that the ANC, by definition, does not depend on the principal quantum number n_r . In Eq. (15) n_r appears as the result of using the shell-model for the bound state wave function $\varphi_{n_A(n_r l_{n_A} j_{n_A})}$. Because of that in such an approach when we use the single-particle neutron bound state wave function both the SPANC and SF depend on n_r . To be accurate, we need to indicate explicitly a dependence of the ANC on n_r in Eqs (15) and (17) also. It would underscore that the ANC determined by Eq. (17) is model-dependent. However, if the assumed shell-model configuration is dominant then the model definition (15) should be accurate and we may disregard the dependence of the ANC on n_r in Eqs (15) and (17).

In the internal matrix element, owing to the presence of the distorted waves, the contribution to the radial matrix element over r_{n_A} in Eq. (14) from small r_{n_A} can be suppressed and the dominant contribution comes from the interval $R_{n_A} - \Delta \leq r_{n_A} \leq R_{n_A}$. In this case in this region the single-particle bound state wave function $\varphi_{n_A(n_r l_{n_A} j_{n_A})}$ is governed by the SPANC $b_{n_r l_{n_A} j_{n_A}}$. Hence, the single-particle bound state wave function and, correspondingly, the internal matrix element $M_{int}^{DW(post)}$ are functionals of the SPANC. To underscore it we rewrite $M_{int}^{TH(post)}$ as

$$M_{int}^{TH(post)}[b_{n_r l_{n_A} j_{n_A}}] = S F_{n_r l_{n_A} j_{n_A}}^{1/2} \tilde{M}_{int}^{TH(post)}[b_{n_r l_{n_A} j_{n_A}}], \quad (18)$$

$$\tilde{M}_{int}^{TH(post)} = \langle \chi_{pF}^{(-)} \varphi_{n_A(n_r l_{n_A} j_{n_A})}[b_{n_r l_{n_A} j_{n_A}}] | \Delta V_{pF} | \Phi_i^{(+)} \rangle \Big|_{r_{n_A} \leq R_{n_A}}. \quad (19)$$

Then the total reaction amplitude can be written as

$$M^{TH(post)} = S F_{n_r l_{n_A} j_{n_A}}^{1/2} \tilde{M}_{int}^{TH(post)}[b_{n_r l_{n_A} j_{n_A}}] + C_{l_{n_A} j_{n_A}} \tilde{M}_{ext}^{TH(post)}. \quad (20)$$

Thus we can rewrite the post amplitude as the sum of the internal matrix element, which is the functional of the SPANC $b_{n_r l_{n_A} j_{n_A}}$, and the external matrix element. The normalization of the internal amplitude is determined by the SF while the normalization of the external

matrix element is determined by the ANC. It is valid for all three approaches, DWBA, ADWA and CDCC.

In the conventional approach the SF is determined by normalization of the theoretical differential cross section to the experimental one at the main stripping peak in the angular distribution.

$$SF_{n_r l_{nA} j_{nA}} = \frac{d\sigma^{exp}/d\Omega}{d\sigma^{TH(post)}/d\Omega}, \quad (21)$$

where $d\sigma^{TH(post)}/d\Omega$ can be DWBA, ADWA or CDCC differential cross sections. In such an approach the result depends on the adopted geometry of the $F = (nA)$ bound state potential, which is, a priori, unknown and usually is taken in the standard region. Assume that one has found a SF using this procedure, then the corresponding ANC can be determined from Eq. (17). The ANC determined in such a way can be quite different from the experimental one [2, 4]. Thus the SF extracted using the conventional approach actually may be determined on the expense of the wrong contribution of the external part, which usually is dominant.

In a combined approach suggested in [1, 2] the SF is extracted using the information about ANC. In this approach the normalization of the external part is fixed using the information about the ANC determined independently from other sources. In a such a way the SF can be determined as the normalization factor of the internal amplitude. To add the information about the ANC into the analysis we rewrite Eq. (20) as

$$M^{TH(post)} = C_{l_{nA} j_{nA}} \left(\frac{\tilde{M}_{int}^{TH(post)}[b_{n_r l_{nA} j_{nA}}]}{b_{n_r l_{nA} j_{nA}}} + \tilde{M}_{ext}^{TH(post)} \right), \quad (22)$$

where we took into account Eq. (17). Equating the theoretical and experimental differential cross sections in the first stripping peak we get

$$(C_{l_{nA} j_{nA}}[b_{n_r l_{nA} j_{nA}}])^2 = \frac{d\sigma^{exp}/d\Omega}{\left| \frac{\tilde{M}_{int}^{TH(post)}[b_{n_r l_{nA} j_{nA}}]}{b_{n_r l_{nA} j_{nA}}} + \tilde{M}_{ext}^{TH(post)} \right|^2}. \quad (23)$$

Thus by comparing the experimental differential cross section and theoretical one we can determine the ANC. Because the right-hand side is a functional of the SPANC $b_{n_r l_{nA} j_{nA}}$ the phenomenological ANC determined from Eq. (23) is also a functional of the SPANC. If $\tilde{M}_{int}^{TH(post)}[b_{n_r l_{nA} j_{nA}}]$ is negligible then the reaction is dominantly peripheral and extracted from Eq. (23) phenomenological ANC has no or little $b_{n_r l_{nA} j_{nA}}$ dependence. In this case the

determined ANC can be considered as an experimental one. Reliability of the determined ANC depends on the adopted reaction theory. Note that in the case of the peripheral reaction the extracted SF in the standard procedure is determined by

$$SF_{n_r l_{nA} j_{nA}} = \frac{d\sigma^{exp}/d\Omega}{(b_{n_r l_{nA} j_{nA}})^2 |\tilde{M}_{ext}^{TH(post)}|^2}. \quad (24)$$

Because $\tilde{M}_{ext}^{TH(post)}$ does not depend on $b_{n_r l_{nA} j_{nA}}$, in the case of the pure peripheral reaction $SF_{n_r l_{nA} j_{nA}} \sim (b_{n_r l_{nA} j_{nA}})^{-2}$.

If a reaction is not peripheral then the phenomenological ANC depends on the SPANC. The stronger this dependence the stronger contribution of the nuclear interior. If in this case the ANC is known, for example determined from a peripheral reaction, then from the intersection of the phenomenological ANC and experimental one,

$$(C_{l_{nA} j_{nA}}[b_{n_r l_{nA} j_{nA}}])^2 = (C_{l_{nA} j_{nA}})^2, \quad (25)$$

we can determine the SPANC $b_{(0)n_r l_{nA} j_{nA}}$, which is solution of Eq. (25), and then from Eq. (17) we can find the SF. The stronger the dependence of $C_{l_{nA} j_{nA}}[b_{n_r l_{nA} j_{nA}}]$ on $b_{n_r l_{nA} j_{nA}}$ the smaller the uncertainty of the determined SF. In practical calculations of the bound state wave function we use the Woods-Saxon potential determined by the geometrical parameters, radius r_0 and diffuseness a . The depth of the potential is adjusted to reproduce the experimental binding energy. The SPANC $b_{n_r l_{nA} j_{nA}}$ is a function of these geometrical parameters of the Woods-Saxon potential and for each given $b_{n_r l_{nA} j_{nA}}$ we can find infinite number of the pair r_0, a generating this SPANC. However, if we fix one of the geometrical parameters, for example diffuseness, then there is a unique correspondence between r_0 and $b_{n_r l_{nA} j_{nA}}$. Then, from Eq. (25) we can determine r_0 or a range of r_0 at which this equation is satisfied.

Once the SPANC has been determined, using Eq. (17) we can immediately find the SF, which does not suffer from the ambiguity of the geometrical parameters of the bound state Woods-Saxon potential. This SF is determined from the internal contribution to the reaction amplitude, while the normalization of the external part is fixed using the experimentally determined ANC. However in the practical applications the experimentally determined ANC has uncertainty caused by the uncertainties of the experimental and theoretical differential cross sections. Due to these uncertainties intersection of $(C_{l_{nA} j_{nA}}[b_{n_r l_{nA} j_{nA}}])^2$ with the experimental $(C_{l_{nA} j_{nA}})^2$ may provide $b_{(0)n_r l_{nA} j_{nA}} \pm \Delta b_{n_r l_{nA} j_{nA}}$, where uncertainty $\Delta b_{n_r l_{nA} j_{nA}}$ is not small compared to $b_{(0)n_r l_{nA} j_{nA}}$. It leads to a bigger uncertainty in the determined SF.

In the standard approach of determination of the SF the information about the ANC is completely disregarded and the SF is determined by adopting standard geometrical parameters, $r_0 = 1.1 - 1.35$ fm and $a = 0.5 - 0.7$ fm. Because the geometrical parameters of the Woods-Saxon potential are chosen arbitrarily the SF extracted in the standard approach are usually determined on the expense of the normalization of the external part. The external part usually dominates or plays an important role up to the deuteron incident energies $E_d \sim 100$ MeV. Hence by a small variation of the external part contribution one can achieve a much bigger variation of the internal part, which gives the main contribution to the SF. The main advantage of the combined method is that it puts serious limitations on the theory by fixing the normalization of the external part of the reaction amplitude. This normalization is governed by the ANC, which can be measured experimentally from peripheral reactions. Hence the normalization of the peripheral amplitude can be fixed experimentally. In this case the SF is determined from the internal contribution to the reaction amplitude. Such a reformulation of the theory puts it on a correct and clear physical basis: the external part is controlled by the ANC and the internal part by the SF. Hence using the combined method, a priori, we can determine an interval of the geometrical parameters and the corresponding SFs keeping the external normalization fixed. Thus in the combined method the reliability of the determined SFs depends on the accuracy of the theory in treating the internal part, which can be compromised. The problem is that the existing approaches, post DWBA, ADWA and CDCC, are based on the three-body model extended by adopting optical potentials and are designed to treat mostly peripheral reactions. However, if we consider the internal region, where a strong coupling of different channels occurs and antisymmetrization effects are important, it is legitimate to ask whether the initial channel wave function $\Phi_i^{(+)}$ used in all the above mentioned methods is adequate to treat the nuclear interior. The combined method can reveal the adequacy of the theory in the internal region.

IV. NUMERICAL RESULTS

Here we present the calculations for three different deuteron stripping reactions on ^{14}C , ^{58}Ni and ^{116}Sn populating the ground states of the final nuclei. Thus we select light, medium and heavier targets. The goal is to demonstrate how the combined method works versus the conventional one. Each reaction is analyzed at two different energies: one is low

so that the reaction is peripheral and the ANC can be determined. Then this ANC is used to analyze the same reaction at higher energy, where the internal contribution becomes more important and the SF is extracted. For the analysis we use three different approaches: DWBA, ADWA and CDCC. Because the SPANC is a function of the geometrical parameters of the bound state potential, in what follows we present the extracted ANCs and SFs as functions of r_0 . Throughout the paper we use the diffuseness $a = 0.65$ fm of the Woods-Saxon potential supporting the neutron bound states in ^{15}C , ^{59}Ni and ^{117}Sn . For the deuteron bound-state potential we adopt the Gaussian one from [11] with the depth 72.15 MeV and radius 1.484 fm. The numerical calculations of the transfer reaction differential cross sections for the (d, p) reactions on ^{14}C and ^{58}Ni are performed using the FRESKO code [13]. For the analysis of the ^{116}Sn reaction was used the TWOFNR [14] code with non-locality corrections for the neutron bound-state and optical potentials. The details of the calculations of the transfer reaction amplitudes are described in [13].

A. Reaction $^{14}\text{C}(d, p)^{15}\text{C}$.

In all the calculations in this section we use the KD optical $N - A$ potentials [6]. In the ADWA the deuteron optical potential is calculated using the KD $N - A$ optical potentials and Johnson-Tandy procedure [8]. In the DWBA calculations we use the Daehnick et al. (Daehnick) global deuteron optical potential [12].

1. Reaction $^{14}\text{C}(d, p)^{15}\text{C}$ at 23.4 MeV.

We start from the low-energy reaction $^{14}\text{C}(d, p)^{15}\text{C}(2s_{1/2})$ at 23.4 MeV. In the case under consideration the binding energy of the transferred neutron in ^{15}C is $\varepsilon_n^{15}\text{C} = 1.218$ MeV. The neutron bound state wave function in the ground state has one node at $r_{nA} > 0$. The adopted optical potential parameters are given in Table I .

In Fig. 1 we present three angular distributions obtained using the DWBA, ADWA and CDCC. We see that all three methods equally well reproduce the first stripping peak. From Fig. 2 it is evident that this reaction is peripheral because variation of the square of the ANC from the central value is about 3%, that is, the ANC changes very little over the broad interval of changing of the radius r_0 of the Woods-Saxon potential supporting the neutron

TABLE I. Optical model potential parameters used in the calculations for the $^{14}\text{C}(d, p)^{15}\text{C}(2s_{1/2})$ reaction at 23.4 MeV. V , r_V and a_V are the depth, radius and diffuseness parameters of the real part, W , r_W , a_W and W_s , r_s , a_s are depth, radius and diffuseness parameters of the volume and surface imaginary parts, respectively, of the optical potential of the standard Woods-Saxon type. Deuteron-target optical potential in the DWBA calculations are of Daehnick et al. (Daehnick) [12]; proton and neutron potentials are all of KD systematics [6]. Potential depths are in MeV and geometry parameters are in fm.

projectile	target	energy	V	r_V	a_V	W	r_W	a_W	W_s	r_s	a_s	Potential type
d	^{14}C	23.4	84.61	1.17	0.749	0.68	1.33	0.659	12.13	1.33	0.659	Daehnick
p	^{14}C	11.7	54.76	1.14	0.676	0.98	1.14	0.676	8.88	1.30	0.526	KD
n	^{14}C	11.7	47.40	1.14	0.676	1.04	1.14	0.676	6.66	1.30	0.542	KD
p	^{15}C	20.8	52.12	1.14	0.676	1.94	1.14	0.676	8.82	1.30	0.527	KD

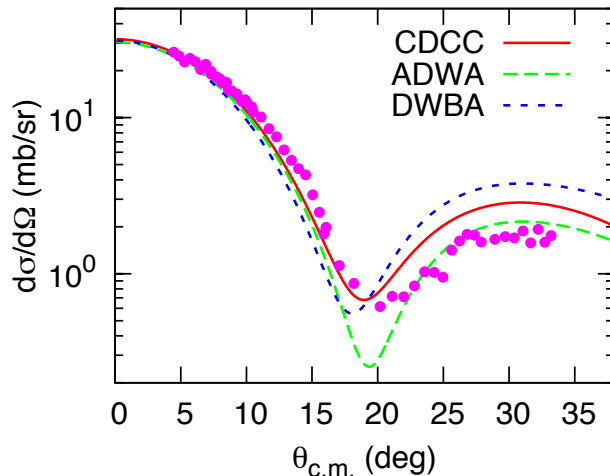


FIG. 1. (Color online) Angular distributions of the DWBA, ADWA and CDCC differential cross sections for the deuteron stripping $^{14}\text{C}(d, p)^{15}\text{C}(2s_{1/2})$ at $E_d = 23.4$ MeV. Blue short and green dashed lines are the post DWBA and ADWA differential cross sections, correspondingly. The solid red line is the post CDCC calculation. The theoretical differential cross sections are normalized to the experimental one at forward angles. Dots are the experimental data from [5].

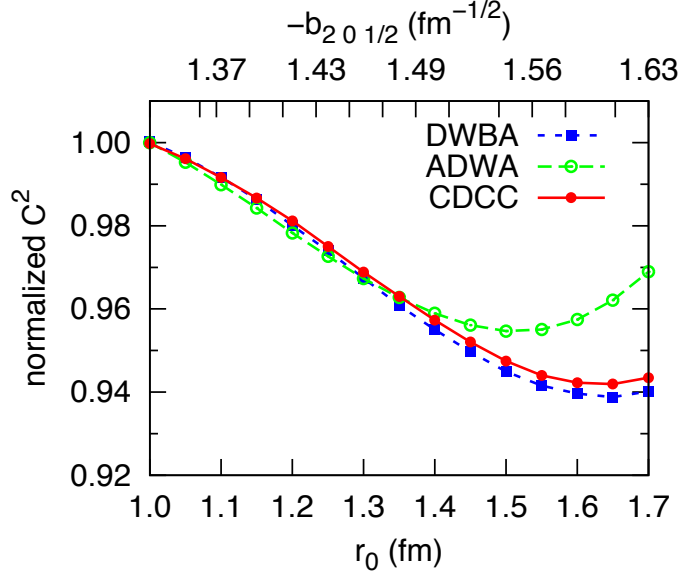


FIG. 2. (Color online) r_0 -dependence of the ANCs normalized to unity at $r_0 = 1$ in the DWBA, ADWA and CDCC for the deuteron stripping $^{14}\text{C}(d, p)^{15}\text{C}(2s_{1/2})$ at $E_d = 23.4$ MeV. Blue rectangular dots and short dashed line is the ANC determined from the DWBA, green open dots and dashed line is the ANC obtained from the ADWA and filled red dots and solid line is the ANC obtained from the CDCC. For simplicity, the subscripts denoting the quantum numbers in the ANC are omitted.

bound state in ^{15}C . The determined square of the ANC from the CDCC calculations is $C_{01/2}^2 = 1.80 \pm 0.2 \text{ fm}^{-1}$. In what follows, for simplicity, we use the ANC keeping in mind that actually we mean the square of ANC.

In Fig. 3 we show the r_0 -dependence of the SFs normalized to unity at $r_0 = 1$ in three different methods, DWBA, ADWA and CDCC. The SFs are calculated using Eq. (17). While the ANC changes very little, the SF varies by $\approx 40\%$ when r_0 varies from $r_0 = 1.0$ fm until $r_0 = 1.7$ fm. Also in this figure (magenta dotted line) we show the r_0 -dependence of the normalized SF in the case of the pure peripheral reaction, $SF \sim 1/(b_{201/2})^2$. The closeness of the extracted SFs to the peripheral line confirms that the reaction is peripheral.

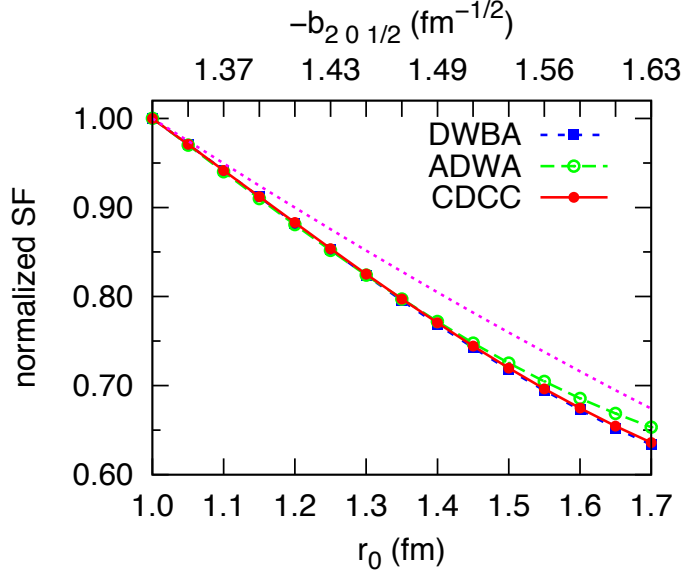


FIG. 3. (Color online) r_0 -dependence of the SFs normalized to unity at $r_0 = 1$ in the DWBA, ADWA and CDCC for the deuteron stripping $^{14}\text{C}(d, p)^{15}\text{C}(2s_{1/2})$ at $E_d = 23.4$ MeV. Blue rectangular dots and short dashed line is the SF determined from the DWBA, open green dots and dashed line is the SF obtained from the ADWA and red filled dots and solid line is the SF obtained from the CDCC. Magenta dotted line is the r_0 -dependence of the normalized SF in the case of pure peripheral reaction. For simplicity, the subscripts denoting the quantum numbers in the SF are omitted.

2. Reaction $^{14}\text{C}(d, p)^{15}\text{C}$ at 60 MeV.

After determining the ANC from the low-energy data now we can apply the combined method to determine the neutron SF in ^{15}C from the analysis of the $^{14}\text{C}(d, p)^{15}\text{C}(2s_{1/2})$ reaction at $E_d = 60$ MeV. The higher energy is selected to get a higher contribution from the nuclear interior, which is more sensitive to the SF. The adopted optical potential parameters are given in Table II.

In Fig. 4 we show the calculated angular distributions for $^{14}\text{C}(d, p)^{15}\text{C}$ at $E_d = 60$ MeV. Because this reaction is measured at higher energy we expect that this reaction is less peripheral than at 23.4 MeV [5].

In Fig 5 we show the r_0 -dependence of the ANCs normalized to unity at $r_0 = 1$ in three different methods, DWBA, ADWA and CDCC. As we see the behavior of the ANC depends on the method used. In [5] the ADWA was used to analyze this reaction at $E_d = 60$ MeV.

TABLE II. Optical model potential parameters used in the calculations for the $^{14}\text{C}(d, p)^{15}\text{C}(2s_{1/2})$ reaction at 60 MeV. Notations are the same as in Table I.

projectile	target	energy	V	r_V	a_V	W	r_W	a_W	W_s	r_s	a_s	Potential type
d	^{14}C	60.0	75.09	1.17	0.811	4.16	1.33	0.659	9.60	1.33	0.659	Daehnick
p	^{14}C	30.0	47.70	1.14	0.676	3.07	1.14	0.676	7.29	1.30	0.526	KD
n	^{14}C	30.0	41.28	1.14	0.676	2.87	1.14	0.676	5.21	1.30	0.542	KD
p	^{15}C	54.9	39.93	1.14	0.676	6.16	1.14	0.676	4.70	1.30	0.527	KD

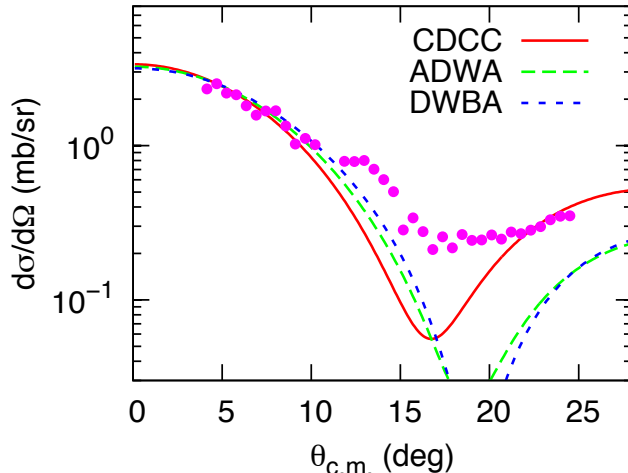


FIG. 4. (Color online) Angular distributions of the DWBA, ADWA and CDCC differential cross sections for the deuteron stripping $^{14}\text{C}(d, p)^{15}\text{C}(2s_{1/2})$ at $E_d = 60$ MeV. Blue short and green dashed lines are the post DWBA and ADWA differential cross sections, correspondingly. The solid red line is the CDCC calculation. The theoretical differential cross sections are normalized to the experimental one at forward angles. Dots are the experimental data from [5].

While in the DWBA the reaction is completely peripheral, it becomes less peripheral within the ADWA and non-peripheral in the CDCC. These observations are confirmed by Fig. 6 in which we show the r_0 -dependence of the SFs. As we can see the SF determined in the DWBA is very close to the peripheral dependence. The ADWA is less peripheral but the CDCC gives the strongest non-peripheral case.

To determine the SF from the 60 MeV data the ADWA was used in [5]. It is understandable now why the combined method failed in [5]. It is because the internal contribution in

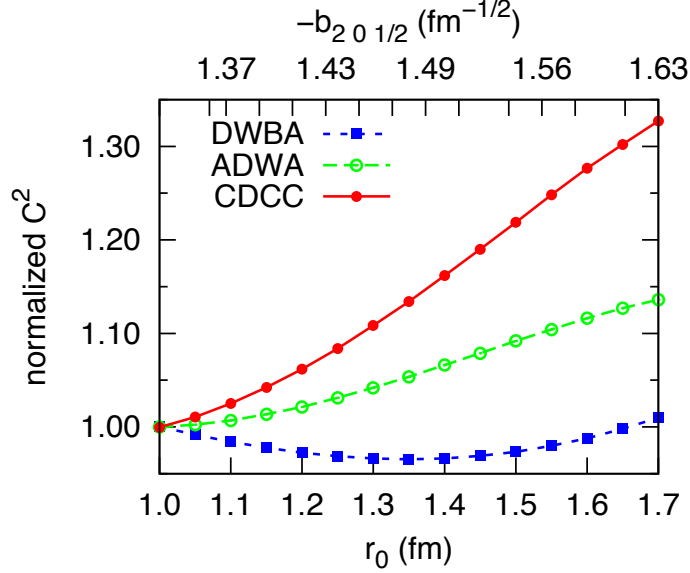


FIG. 5. (Color online) r_0 -dependence of the ANCs normalized to unity at $r_0 = 1$ in the DWBA, ADWA and CDCC for the deuteron stripping $^{14}\text{C}(d, p)^{15}\text{C}(2s_{1/2})$ at $E_d = 60$ MeV. Blue rectangular dots and short dashed line is the ANC determined from the DWBA, green open dots and dashed line is the ANC obtained from the ADWA and filled red dots and solid line is the ANC obtained from the CDCC. For simplicity, the subscripts denoting the quantum numbers in the ANC are omitted.

the ADWA was not significant enough. Evidently that the CDCC method with more significant non-peripherality among all three methods is the best candidate to apply the combined method.

Our previous observations about the peripheral character of the low-energy reaction and important contribution of the internal region at 60 MeV are confirmed by Fig. 7, where the normalized differential cross section R_x is shown as a function of r_{nA}^{min} and r_{nA}^{max} . To get the dependence on r_{nA}^{min} the neutron bound state wave function in ^{15}C is cut at $r_{nA} < r_{nA}^{min}$. Hence r_{nA}^{min} is the lower limit of the radial matrix element over r_{nA} . To determine the dependence of R_x on r_{nA}^{max} we cut the neutron bound state wave function at $r_{nA} > r_{nA}^{max}$. In this case r_{nA}^{max} becomes the upper limit in the radial matrix element over r_{nA} . The normalized differential cross section R_x is determined as the ratio of the differential cross section calculated at the peak of the angular distribution as the function of r_{nA}^{min} or r_{nA}^{max} to the full differential cross section also calculated at the peak of the angular distribution. Figure 7 clearly shows that the reaction under consideration is peripheral at 23.4 MeV and non-peripheral at 60 MeV.

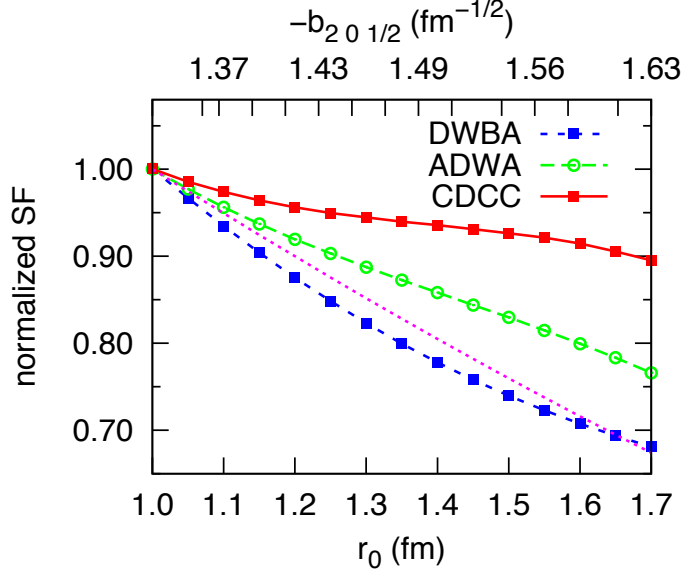


FIG. 6. (Color online) r_0 -dependence of the SFs normalized to unity at $r_0 = 1$ in the DWBA, ADWA and CDCC for the deuteron stripping $^{14}\text{C}(d, p)^{15}\text{C}(2s_{1/2})$ at $E_d = 60$ MeV. Blue rectangular dots and short dashed line is the SF determined from the DWBA, open green dots and dashed line is the SF obtained from the ADWA and red filled dots and solid line is the SF obtained from the CDCC. Magenta dotted line is the r_0 -dependence of the normalized SF in the case of pure peripheral reaction. For simplicity, the subscripts denoting the quantum numbers in the SF are omitted.

For example, we see that at 23.4 MeV R_x changes very little as function of r_{nA}^{min} (green dashed line) until $r_{nA}^{min} \sim 4.5$ fm, that is, the contribution to the reaction amplitude from the internal region is suppressed. The red solid line showing the dependence of R_x on r_{nA}^{max} confirms that the significant contribution to the matrix element begins at $r_{nA}^{max} > 5$ fm, that is, the reaction is peripheral. Meantime at 60 MeV we observe quite a different behavior of R_x . The dependence on r_{nA}^{max} (blue dashed line) shows that the internal region between 3 and 6 fm plays an important role, which is different from the 23.4 MeV case.

In Fig 8 we compare the ANCs extracted within the CDCC method from the analysis of 23.4 MeV and 60 MeV data. Owing to the 11% uncertainty of the determined ANCs [5], the region of the overlapping of the ANCs from 23.4 and 60 MeV data is quite wide. We select this region as the interval $1.10 \text{ fm} \leq r_0 \leq 1.60 \text{ fm}$ (this radii are realistically acceptable for the bound state Woods-Saxon potentials) .

Note that the corresponding interval in the SPANC is $1.37 \leq |b_{201/2}| \leq 1.58$. The central

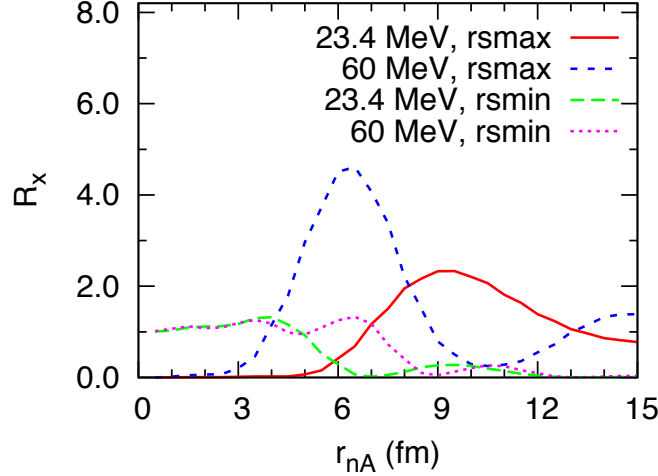


FIG. 7. (Color online) (Color online) Dependence of the normalized CDCC differential cross sections R_x on r_{nA} for the deuteron stripping $^{14}\text{C}(d, p)^{15}\text{C}(2s_{1/2})$ at $E_d = 23.4$ and 60 MeV. Green dashed and magenta dotted line are R_x at 23.4 and 60 MeV, correspondingly. To get these R_x we calculated the post CDCC differential cross section at the peak of the angular distribution. The radial integral over r_{nA} is calculated for $r_{nA}^{min} \leq r_{nA} < \infty$. The calculated differential cross section is normalized to the full differential cross section calculated at the peak of the angular distribution. Similarly, solid red and blue short dashed lines are the post CDCC R_x calculated at 23.4 and 60 MeV, correspondingly, in which the radial integral over r_{nA} is calculated in the interval $0 \leq r_{nA} \leq r_{nA}^{max}$. Again the calculated differential cross sections are normalized to the full differential cross sections at the corresponding energies. Hence, r_{nA} on the abscissa is r_{nA}^{min} for the green dashed and magenta dotted lines and r_{nA}^{max} for the solid red and blue short dashed lines.

value is $r_0 = 1.35$ fm, which corresponds to the square of the ANC $C_{01/2}^2 = 1.80 \pm 0.2 \text{ fm}^{-1}$, which is in a nice agreement with the value found in [5]. Despite the wide interval of r_0 , owing to the non-peripheral character of the reaction at 60 MeV, the SF (the solid red line in Fig. 6) does not change much and the combined analysis of the peripheral reaction at 23.4 MeV and non-peripheral at 60 MeV results in $\text{SF}_{201/2} = 0.82 \pm 0.03$. Thus using the CDCC method we are able to determine a reasonable SF under the condition that the experimental ANC governs the normalization of the peripheral part of the reaction amplitude. That is what we call compatibility of the ANC and the SF. This result demonstrates the power of the combined method when the reaction theory works. We summarize the results of the analysis in this section:

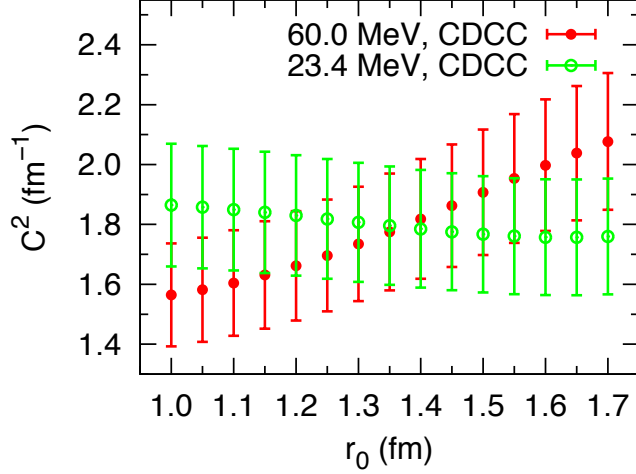


FIG. 8. (Color online) Comparison of the r_0 dependence of the ANCs in the CDC for the deuteron stripping $^{14}\text{C}(d, p)^{15}\text{C}(2s_{1/2})$ at $E_d = 23.4$ MeV and 60 MeV. Open green dots is the ANC r_0 -dependence from 23.4 MeV reaction and solid red dots is the ANC r_0 dependence from 60 MeV reaction. For simplicity, the subscripts denoting the quantum numbers in the ANC are omitted.

- (1) The important part of the analysis is the application of the CDCC method.
- (2) The determined SF is very reasonable and has small uncertainty due to the non-peripheral character of the reaction at 60 MeV.
- (3) The SF and ANC are compatible because for the whole interval of the determined SF the corresponding ANC is within the uncertainty interval (see Fig. 8).
- (4) The accuracy of the determined SF is determined by the accuracy of the reaction model in the nuclear interior. In the case under consideration the main contribution to the reaction amplitude at 60 MeV comes from the internal region close to the surface (3 – 5 fm), surface region (5–7 fm) and peripheral region (> 7 fm). Thus although the reaction is not peripheral at 60 MeV the contribution of the deep interior is still significantly weakened. In the internal region close to the surface the CDCC approach turns out to be acceptable making the ANC and SF compatible.

B. Reaction $^{58}\text{Ni}(d, p)^{59}\text{Ni}$.

We apply now the combined method for the analysis of the deuteron stripping $^{58}\text{Ni}(d, p)^{59}\text{Ni}(2p_{3/2})$ at $E_d = 10$ MeV and 56 MeV. The low-energy case is selected to get the ANC and then to

use this ANC to determine the neutron SF in ^{59}Ni from the higher energy reaction at 56 MeV. Note that the final bound state wave function, as in the previous case, has one node at $r_{nA} > 0$ but the neutron is much stronger bound than in ^{15}C . In all the calculations in this section we use the KD optical $N - A$ potentials [6]. In the ADWA the deuteron optical potential is calculated using the KD $N - A$ optical potentials and Johnson-Tandy procedure [8]. In the DWBA calculations we use the Daehnick et al. (Daehnick) global deuteron optical potential [12].

1. Reaction $^{58}\text{Ni}(d, p)^{59}\text{Ni}$ at 10 MeV.

The adopted optical potential parameters are given in Table III. In Fig. 9 we present three angular distributions obtained using the DWBA, ADWA and CDCC for $E_d = 10$ MeV. We see that all three methods reproduce the first stripping peak although the CDCC and ADWA agree with the experimental data better than the DWBA.

TABLE III. Optical model potential parameters used in the calculations of the $^{58}\text{Ni}(d, p)^{59}\text{Ni}(2p_{3/2})$ reaction at 10 MeV . Notations are the same as in Table I.

projectile	target	energy	V	r_V	a_V	W	r_W	a_W	W_s	r_s	a_s	Potential type
d	^{58}Ni	10.0	92.27	1.17	0.726	0.12	1.33	0.786	12.34	1.33	0.786	Daehnick
p	^{58}Ni	5.0	57.39	1.20	0.669	0.39	1.20	0.669	6.86	1.28	0.549	KD
n	^{58}Ni	5.0	51.39	1.20	0.669	0.45	1.20	0.669	6.97	1.28	0.535	KD
p	^{59}Ni	16.7	52.86	1.20	0.669	1.34	1.20	0.669	8.09	1.28	0.549	KD

From Fig. 10 we can conclude that, despite high neutron binding energy $\epsilon_n^{59\text{Ni}} = 8.999$ MeV, in the ADWA and CDCC the ANC changes very little over the broad interval of the variation of r_0 (or the SPANC $b_{213/2}$) of the Woods-Saxon potential supporting the neutron bound state in ^{59}Ni . The DWBA shows a less peripheral character of the reaction than ADWA and CDCC.

In Fig. 11 we present the r_0 -dependence of the SFs normalized to unity at $r_0 = 1$ in three different methods, DWBA, ADWA and CDCC, determined from the reaction at $E_d = 10$ MeV. The SFs are calculated using Eq. (17). Also in this figure (magenta dotted line)

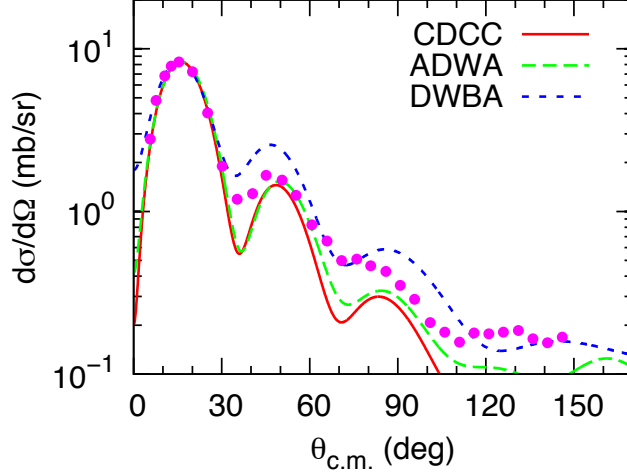


FIG. 9. (Color online) Angular distributions of the DWBA, ADWA and CDCC differential cross sections for the deuteron stripping $^{58}\text{Ni}(d, p)^{59}\text{Ni}(2p_{3/2})$ at $E_d = 10$ MeV. Notations are the same as in Fig. 1. Dots are the experimental data from [15]. All the calculated angular distributions are normalized to the experimental one at the first stripping peak.

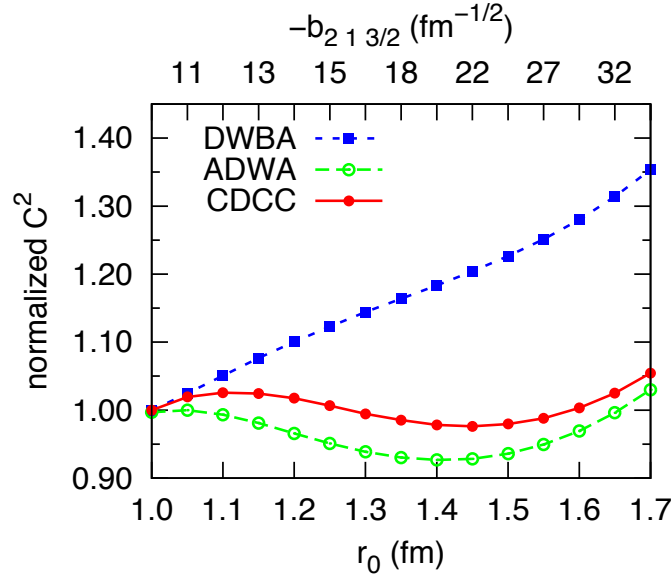


FIG. 10. (Color online) r_0 -dependence of the ANC's normalized to unity at $r_0 = 1$ in the DWBA, ADWA and CDCC for the deuteron stripping $^{58}\text{Ni}(d, p)^{59}\text{Ni}(2p_{3/2})$ at $E_d = 10$ MeV. Notations are the same as in Fig. 2. For simplicity, the subscripts denoting the quantum numbers in the ANC are omitted.

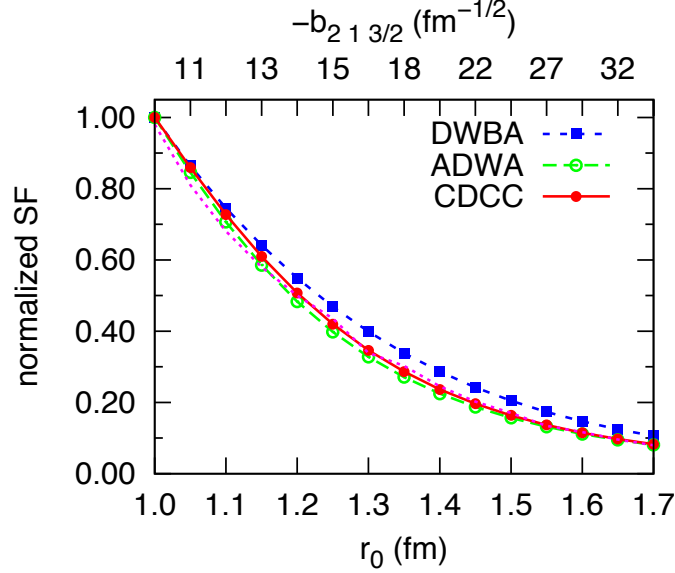


FIG. 11. (Color online) r_0 -dependence of the SFs normalized to unity at $r_0 = 1$ in the DWBA, ADWA and CDCC for the deuteron stripping $^{58}\text{Ni}(d, p)^{59}\text{Ni}(2p_{3/2})$ at $E_d = 10$ MeV. Notations are the same as in Fig. 3. For simplicity, the subscripts denoting quantum numbers are omitted in the SF.

we show the r_0 -dependence of the normalized SF for the pure peripheral reaction, which is given by $SF_{213/2} \sim 1/(b_{213/2})^2$. Owing to the peripheral character of the reaction in the ADWA and CDCC, the corresponding SFs are very close to the one expected in the case of the totally peripheral reaction. Because in the DWBA the reaction at $E_d = 10$ MeV is less peripheral, the r_0 -dependence of the extracted SF slightly deviates from the peripheral line.

From the analysis of the data at 10 MeV we determine the square of the ANC for the neutron removal from ^{59}Ni as $C_{13/2}^2 = 111.7 \pm 12 \text{ fm}^{-1}$ assuming a 10% uncertainty for the ANC.

2. Reaction $^{58}\text{Ni}(d, p)^{59}\text{Ni}$ at 56 MeV

After determining the ANC from the low-energy data we can apply the combined method to determine the neutron SF in ^{59}Ni from the analysis of the $^{58}\text{Ni}(d, p)^{59}\text{Ni}(2p_{3/2})$ reaction at $E_d = 56$ MeV. The adopted optical potential parameters are given in Table IV.

In Fig. 12 we present the angular distributions obtained using DWBA, ADWA and CDCC. The DWBA fails to reproduce the experimental angular distribution while both

TABLE IV. Optical model potential parameters used in the calculations for the $^{58}\text{Ni}(d, p)^{59}\text{Ni}(2p_{3/2})$ reaction at 60 MeV. Notations are the same as in Table I.

projectile	target	energy	V	r_V	a_V	W	r_W	a_W	W_s	r_s	a_s	Potential type
d	^{58}Ni	56.0	80.31	1.17	0.804	3.68	1.33	0.786	9.98	1.33	0.786	Daehnick
p	^{58}Ni	28.0	48.21	1.20	0.669	2.62	1.20	0.669	6.90	1.28	0.549	KD
n	^{58}Ni	28.0	43.28	1.20	0.669	2.49	1.20	0.669	6.21	1.28	0.535	KD
p	^{59}Ni	61.9	36.82	1.20	0.669	6.72	1.20	0.669	3.60	1.28	0.549	KD

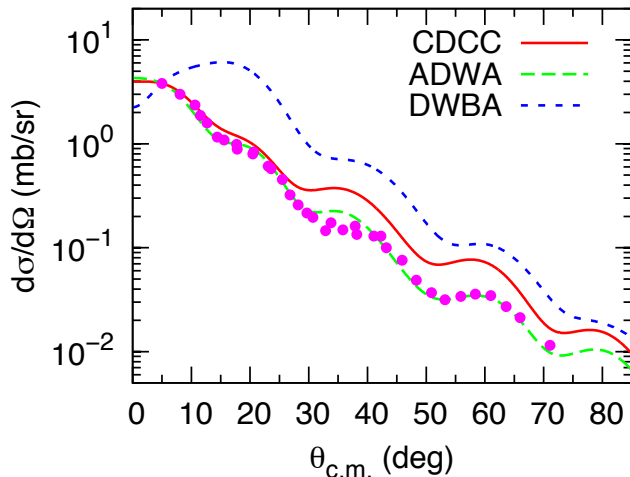


FIG. 12. (Color online) Angular distributions of the DWBA, ADWA and CDCC differential cross sections for the deuteron stripping $^{58}\text{Ni}(d, p)^{59}\text{Ni}(2p_{3/2})$ at $E_d = 56$ MeV. Notations are the same as in Fig. 1. Dots are the experimental data from [16, 17]. The calculated angular distributions are normalized to the experimental one at the forward peak.

ADWA and CDCC reproduce the first stripping peak quite well. In what follows for the analysis of 56 MeV data we use only ADWA and CDCC method.

In Fig. 13 we compare the r_0 -dependence of the post ADWA normalized differential cross sections on r_A^{min} and r_{nA}^{max} at 10 and 56 MeV.

Fig. 13 clearly shows that the reaction under consideration is peripheral at 10 MeV and non-peripheral at 56 MeV. For example, we see that at 10 MeV R_x changes very little as function of r_{nA}^{min} (green dashed line) until $r_{nA}^{min} \simeq 6$ fm, that is, the main contribution to the reaction amplitude comes from the peripheral region. The red solid line showing the

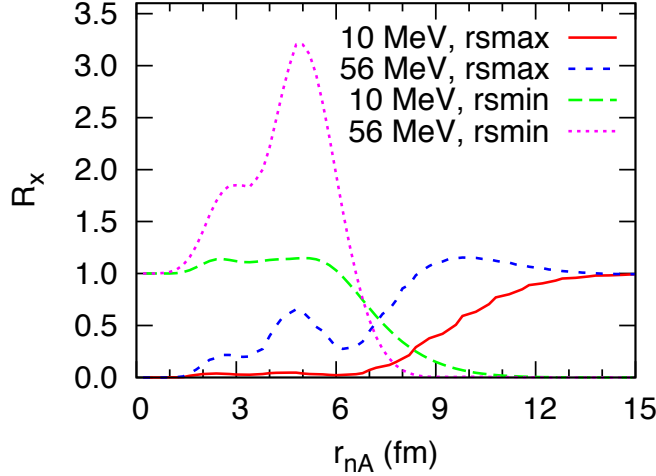


FIG. 13. (Color online) (Color online) Dependence of the normalized ADWA differential cross sections R_x on r_{nA} for the deuteron stripping $^{58}\text{Ni}(d, p)^{59}\text{Ni}(1d_{3/2})$ at $E_d = 10$ and 56 MeV. Green dashed and magenta dotted line are R_X at 10 and 56 MeV, correspondingly. To get these R_x we calculated the post ADWA differential cross section at the peak of the angular distribution. The radial integral over r_{nA} is calculated for $r_{nA}^{min} \leq r_{nA} < \infty$. The calculated differential cross section is normalized to the full differential cross section. Similarly, solid red and blue short dashed lines are the post ADWA R_X calculated at 10 and 56 MeV, correspondingly, in which the radial integral over r_{nA} is calculated in the interval $0 \leq r_{nA} \leq r_{nA}^{max}$. Again the calculated differential cross sections are normalized to the full differential cross sections at the corresponding energies. Hence, r_{nA} on the abscissa is r_{nA}^{min} for the green dashed and magenta dotted lines and r_{nA}^{max} for the solid red and blue short dashed lines.

dependence of R_x on r_{nA}^{max} confirms that the significant contribution to the matrix element begins at $r_{nA}^{max} > 6$ fm. Meantime at 56 MeV we observe quite a different behavior of R_x . The dependence on r_{nA}^{min} (magenta dotted line) shows that the internal region between 1 and 6 fm plays an important role what is drastically different from the 10 MeV case.

In Fig. 14 we present the r_0 -dependence of the ANCs normalized to unity at $r_0 = 1$ in the ADWA and CDCC. As we see the ANC changes very quickly as function of r_0 (or $b_{213/2}$), that is, the reaction at 56 MeV is not peripheral (compare with Fig. 10 for 10 MeV). In Fig. 15 we present the r_0 -dependence of the SFs normalized to unity at $r_0 = 1$ in the ADWA and CDCC for 56 MeV data. The non-peripheral character of the reaction at 56 MeV now is seen in the deviation of the SF from the pure peripheral line although we would expect this

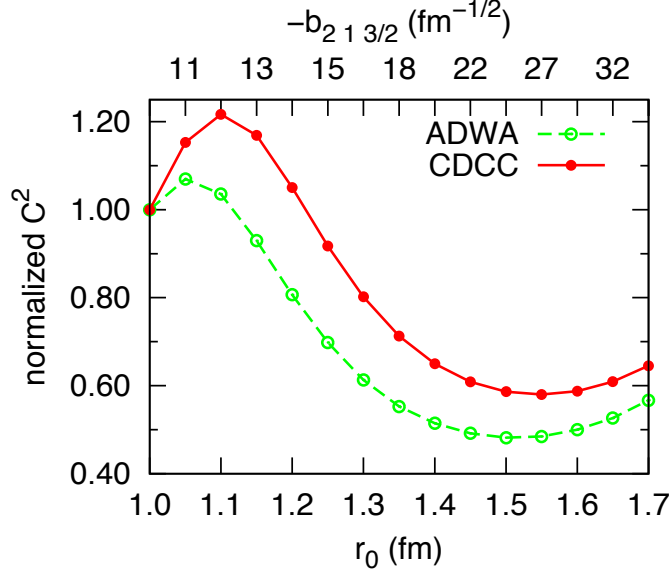


FIG. 14. (Color online) r_0 -dependence of the ANCs normalized to unity at $r_0 = 1$ in the ADWA and CDCC for the deuteron stripping $^{58}\text{Ni}(d, p)^{59}\text{Ni}(2p_{3/2})$ at $E_d = 56$ MeV. Notations are the same as in Fig. 2. For simplicity, the subscripts denoting quantum numbers are omitted in the ANC.

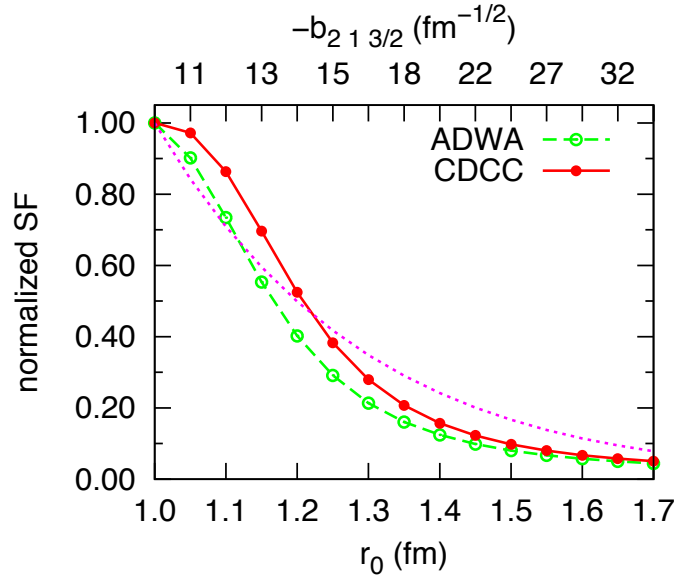


FIG. 15. (Color online) r_0 - dependence of the normalized to unity at $r_0 = 1$ SFs in the ADWA and CDCC for the deuteron stripping $^{58}\text{Ni}(d, p)^{59}\text{Ni}(2p_{3/2})$ at $E_d = 56$ MeV. Notations are the same as in Fig. 3. For simplicity, the subscripts denoting quantum numbers are omitted in the SF.

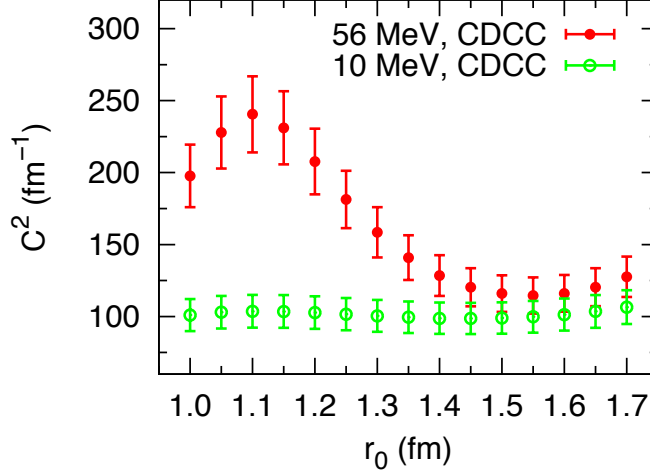


FIG. 16. (Color online) Comparison of r_0 -dependence of the ANCs in the CDCC for the deuteron stripping $^{58}\text{Ni}(d, p)^{59}\text{Ni}(2p_{3/2})$ at $E_d = 10$ MeV and 56 MeV. Green dots is the ANC r_0 -dependence from 10 MeV reaction and red dots from 56 MeV. For simplicity, in the ANC the subscripts denoting quantum numbers are omitted.

deviation to be much stronger. Presumably it demonstrates that, when the nuclear interior becomes more significant, the CDCC method is not accurate and in this case a microscopic approach is required to calculate the internal region contribution more accurately. In Figs. 16 and 17 we compare the ANCs determined from the CDCC and ADWA analysis of the low-energy data at 10 MeV and higher energy data at 56 MeV. By definition, the neutron ANC does not depend on the geometry of the neutron bound-state potential as it is the case for the peripheral 10 MeV reaction (green open dots). For 56 MeV we have a strong dependence of the extracted ANC on r_0 what reflects a non-peripheral character of the reaction. This dependence of the ANC on r_0 allows us to identify the interval of r_0 at which the ANCs determined from 10 and 56 MeV data coincide. It constitutes the combined method of determination of the SF, which can be determined from Eq. (17) once we know r_0 and, hence, the SPANC $b_{213/2}$. From Figs 16 and 17 we see that only in the CDCC there is the region $1.45 \leq r_0 \leq 1.70$ fm corresponding to $22.1 \leq -b_{213/2} \leq 35.40$ fm $^{-1/2}$, where the ANCs from both data do overlap. That is why we analyze only the CDCC calculations. The ANC determined in the CDCC from the 10 MeV data (see Fig 16) is $C_{13/2}^2 = 100 \pm 10$ fm $^{-1}$. From the overlapping region of the ANCs at 10 and 56 MeV data, $1.45 \leq r_0 \leq 1.70$, using Eq. (17) we find that $0.08 \leq SF_{213/2} \leq 0.21$. When determining this interval of the

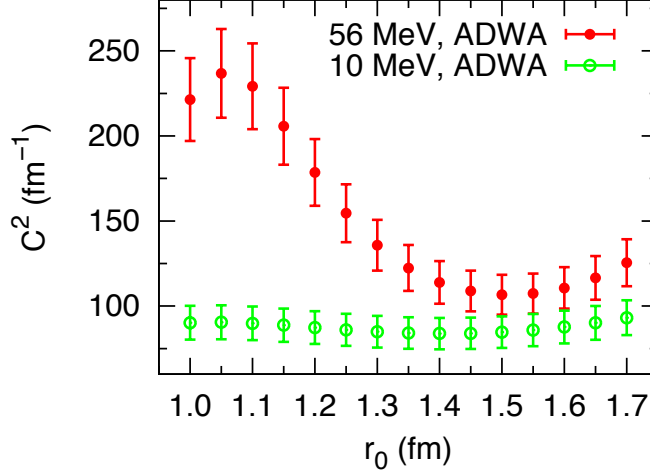


FIG. 17. (Color online) Comparison of the r_0 -dependence of the ANCs in the ADWA for the deuteron stripping $^{58}\text{Ni}(d, p)^{59}\text{Ni}(2p_{1/2})$ at $E_d = 10$ MeV and 56 MeV. Green open dots is the ANC r_0 -dependence from 10 MeV reaction and red solid dots is the ANC from 56 MeV. For simplicity, in the ANC the subscripts denoting quantum numbers are omitted.

SF we fixed the normalization of the peripheral part in terms of the ANC extracted from the 10 MeV data. We find that the combined method provides significantly lower SF than that determined in the standard approach [16, 17], in which a standard geometry of the neutron bound-state potential in ^{59}Ni $r_0 = 1.25$ fm and diffuseness $a = 0.65$ fm was used and the determined SF using the DWBA was in the interval $0.38 - 0.54$.

Let us see what we would get if we use the CDCC and the standard approach to get the SF from the analysis of the data at 56 MeV. In the standard approach the SF is obtained by the normalization of the CDCC differential cross section, calculated using the standard geometry for the neutron bound-state potential in ^{59}Ni , to the experimental one at the forward peak of the angular distribution. Then for the SF we get $SF_{213/2} = 0.77$, which is significantly higher than the value obtained in the combined method. But the corresponding ANC (see the red solid line in Fig. 16 at $r_0 = 1.25$ fm) is $C_{13/2}^2 = 181 \text{ fm}^{-1}$, that is, about 80% higher than the value obtained from the peripheral reaction at 10 MeV. Now we understand that the higher value of the SF in the standard approach is determined on the expense of a significant overestimation of the normalization of the peripheral part of the reaction amplitude, which is governed by the ANC.

We can make some additional conclusion about the internal part of the reaction ampli-

tude. The drop of the ANC as function of r_0 (or, equivalently, $b_{213/2}$) allows us to conclude from Eq. (23) that there is destructive interference between the internal and external amplitudes. The external part does not depend on $b_{213/2}$ and dominates over the internal part. Hence the decrease of the ANC with increase of $b_{213/2}$ is the result of the decrease of the internal part what increases the denominator in Eq. (23) (for the destructive interference of the external and internal parts). A too large ANC obtained from Eq. (23) at the standard geometry $r_0 = 1.25$ fm and diffuseness $a = 0.65$ fm is the result of the overestimation of the internal part in the CDCC (and also in the ADWA). Thus the conventional CDCC method does not provide an accurate contribution of the nuclear interior what is revealed only after application of the combined method. As the result the extracted SF is too small.

The failure of the analysis is related with the fact that now, owing to the high neutron binding energy, the contribution of the deep internal part is much stronger than in the case of ^{15}C and the CDCC theory turns out to be inadequate in treating the internal part. The failure of the CDCC method to treat the nuclear interior is understandable: the CDCC method is a reasonable approximation for the three-body model, which can be valid for the analysis of the nuclear exterior, but not for the treatment of the nuclear interior in which the coupling of channels is important. Correct evaluation of the nuclear interior contribution requires a microscopic many-body approach.

Thus in the case under consideration we observe incompatibility of the ANC and SF. If we use the standard geometry, as in the previous publications [16, 17], we obtain a reasonable SF from the 56 MeV data on the expense of the wrong ANC, which turns out to be significantly higher than the experimental value. If we include the information about the experimental ANC then the determined SF becomes too low. That is the meaning of the incompatibility of the ANC and SF in the combined analysis of the low and higher energy data. The combined method reveals a flaw in the nuclear interior treatment in the contemporary nuclear reaction theory, which is hidden in the standard approach.

C. Reaction $^{116}\text{Sn}(d, p)^{117}\text{Sn}$.

We apply now the combined method for the analysis of the deuteron stripping $^{116}\text{Sn}(d, p)^{117}\text{Sn}$ at $E_d = 12.2$ MeV and 79.2 MeV. The low-energy case is selected to get the ANC and then to use this ANC to determine the neutron SF in ^{117}Sn from the higher energy reaction at

79.2 MeV. In the case under consideration the neutron binding energy in $^{117}\text{Sn}(3s_{1/2})$ is 6.943 MeV. The neutron bound state wave function has two nodes at $r_{nA} > 0$. We find that for the reaction under consideration the CH89 optical potentials work better than KD ones. For the analysis we use the finite Johnson-Tandy ADWA [8] with non-locality corrections in the neutron bound-state and optical potentials with the TWOFNR code [14]. We have found that the non-locality corrections are important. That is why we present below only the ADWA calculations performed with non-local effects using the TWOFNR code. In all the calculations only CH89 optical potentials were used.

1. Reaction $^{116}\text{Sn}(d, p)^{117}\text{Sn}$ at 12.2 MeV.

The adopted optical potential parameters are given in Table V.

TABLE V. Optical model potential parameters used in the calculations for the $^{116}\text{Sn}(d, p)^{117}\text{Sn}(3s_{1/2})$ reaction at 12.2 MeV. Notations are the same as in Table I. Here the proton and neutron optical potentials are CH89 systematics [7].

projectile	target	energy	V	r_V	a_V	W	r_W	a_W	W_s	r_s	a_s	Potential type
p	^{116}Sn	6.1	59.90	1.22	0.661	0.37	1.22	0.661	7.63	1.27	0.579	CH89
n	^{116}Sn	6.1	48.43	1.22	0.661	0.41	1.22	0.661	6.12	1.27	0.525	CH89
p	^{117}Sn	16.8	55.30	1.22	0.660	1.18	1.22	0.660	8.86	1.27	0.580	CH89

In Fig. 18 we present the angular distribution obtained using the ADWA for $E_d = 12.2$ MeV. From Fig. 19 we can conclude that, despite the high neutron binding energy $\varepsilon_n^{117}\text{Sn} = 6.943$ MeV, in the ADWA with the non-local potentials the ANC changes very little over the broad interval $1.0 \leq r_0 \leq 1.7$ fm of the radial parameter (or the SPANC $b_{301/2}$) of the Woods-Saxon potential supporting the neutron bound state in ^{117}Sn . Hence we can conclude that at 12.2 MeV the reaction is peripheral.

In Fig. 20 we present the r_0 -dependence of the SFs normalized to unity at $r_0 = 1$ in the ADWA determined from the reaction at $E_d = 12.2$ MeV. The SF is calculated using Eq. (17). Also in this figure (magenta dotted line) we show the r_0 -dependence of the normalized SF for the pure peripheral reaction, which is given by $SF_{301/2} \sim 1/(b_{301/2})^2$. From the

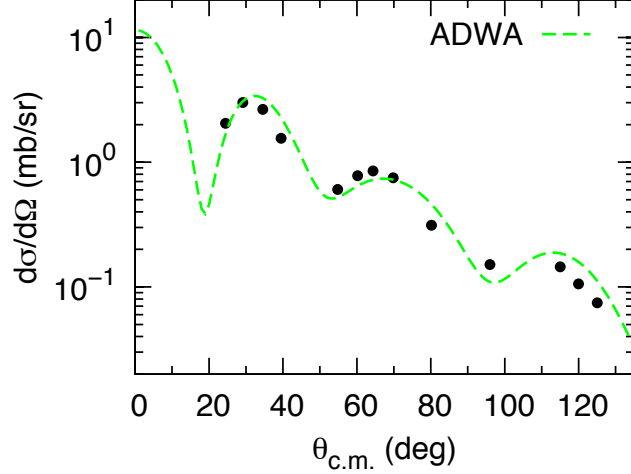


FIG. 18. (Color online) The ADWA differential cross sections for the deuteron stripping $^{116}\text{Sn}(d, p)^{117}\text{Sn}(3s_{1/2})$ at $E_d = 12.2$ MeV - green dashed line. Black dots are the experimental data from [18]. The calculated angular distribution is normalized to the experimental one at the first measured peak.

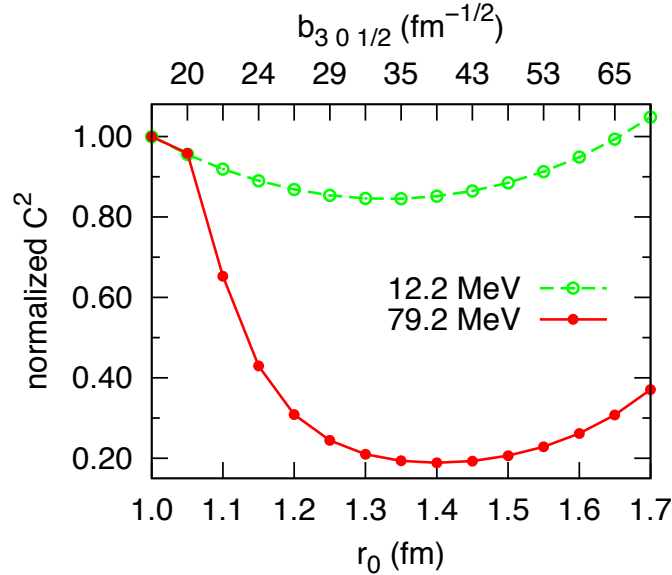


FIG. 19. (Color online) r_0 -dependence of the ANC normalized to unity at $r_0 = 1$ in the ADWA for the deuteron stripping $^{116}\text{Sn}(d, p)^{117}\text{Sn}(3s_{1/2})$ at $E_d = 12.2$ MeV- green open circles and dashed line. The filled dots and solid red line is the r_0 -dependence of the normalized ANC obtained from 79.2 MeV data. For simplicity, in the ANC the subscripts denoting quantum numbers are omitted.

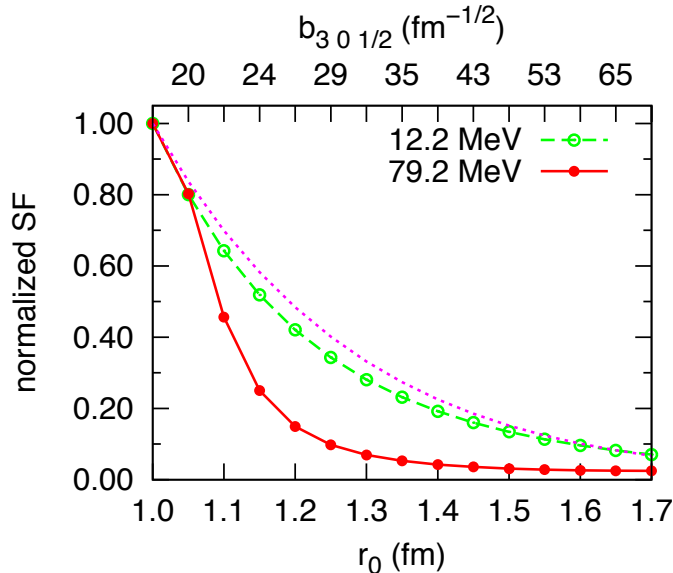


FIG. 20. (Color online) r_0 -dependence of the normalized to unity at $r_0 = 1$ SF in the ADWA for the deuteron stripping $^{116}\text{Sn}(d, p)^{117}\text{Sn}(3s_{1/2})$ at $E_d = 12.2$ MeV is shown by the green open dots and dashed line. The filled dots and solid red line is the r_0 -dependence of the normalized SF obtained from 79.2 MeV data. Magenta dotted line is the r_0 -dependence of the normalized SF in the case of pure peripheral reaction. For simplicity, in the SF the subscripts denoting quantum numbers are omitted.

analysis of the data at 12.2 MeV we determine the ANC for the neutron removal from ^{117}Sn as $C_{03/2}^2 = 310 \pm 30 \text{ fm}^{-1}$ assuming a 10% uncertainty for the ANC.

2. Reaction $^{116}\text{Sn}(d, p)^{117}\text{Sn}$ at 79.2 MeV.

After determining the ANC from the low-energy data now we can apply the combined method to determine the neutron SF in ^{116}Sn from the analysis of the $^{116}\text{Sn}(d, p)^{117}\text{Sn}(3s_{1/2})$ reaction at $E_d = 79.2$ MeV. The adopted optical potential parameters are given in Table VI.

In Fig. 21 we compare the calculated angular distribution in the ADWA with the experimental one [19]. We see that inclusion of all non-locality effects improves the agreement with the experimental data at forward angles. We can conclude from Figs 19 and 20, in which the r_0 -dependence of the normalized ANCs and SFs for 12.2 and 79.2 MeV data are shown, that clearly the reaction at 79.2 MeV is not peripheral.

TABLE VI. Optical model potential parameters used in the calculations for the $^{116}\text{Sn}(d, p)^{117}\text{Sn}(3s_{1/2})$ reaction at 79.2 MeV. Notations are the same as in Table I. Here the proton and neutron optical potentials are CH89 systematics [7].

projectile	target	energy	V	r_V	a_V	W	r_W	a_W	W_s	r_s	a_s	Potential type
p	^{116}Sn	39.6	47.06	1.20	0.690	2.78	1.24	0.690	7.12	1.24	0.690	CH89
n	^{116}Sn	39.6	39.25	1.20	0.690	4.46	1.24	0.690	3.58	1.24	0.690	CH89
p	^{117}Sn	83.3	34.08	1.20	0.690	6.98	1.24	0.690	3.65	1.24	0.690	CH89

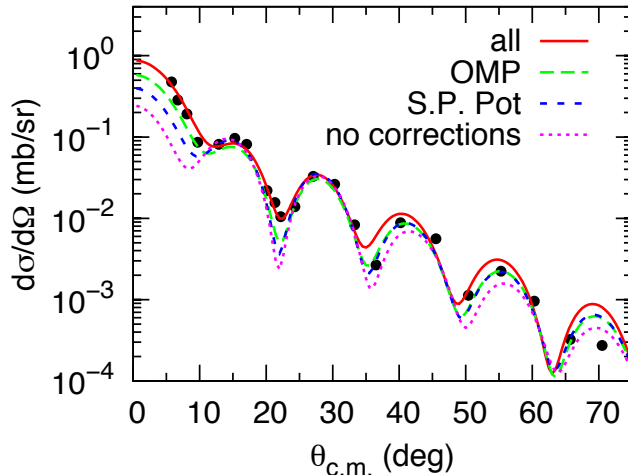


FIG. 21. (Color online) Angular distribution of the ADWA differential cross sections for the deuteron stripping $^{116}\text{Sn}(d, p)^{117}\text{Sn}(3s_{1/2})$ at $E_d = 79.2$ MeV. ADWA calculations without any non-locality effects is the magenta dotted line. ADWA calculations with non-locality effects in the neutron bound state potential is presented by the blue short dashed line. The green dashed line shows the ADWA calculations with the non-local corrections in the optical potentials. Finally the solid red line is the ADWA angular distribution with all non-locality effects included, which is normalized to the experimental one at the forward peak. The same normalization factor was applied to the three other curves. Black dots are the experimental data from [19].

In Fig. 22 we compare the dependence of the post ADWA normalized differential cross sections on r_{nA}^{min} and r_{nA}^{max} at 12.2 and 79.2 MeV. The dependence on r_{nA}^{min} at 12.2 MeV (green dashed line) confirms that the reaction is peripheral because R_x changes very little until $r_{nA}^{min} \approx 7.5$ fm. The peripheral character of the reaction at 12.2 MeV also is evident

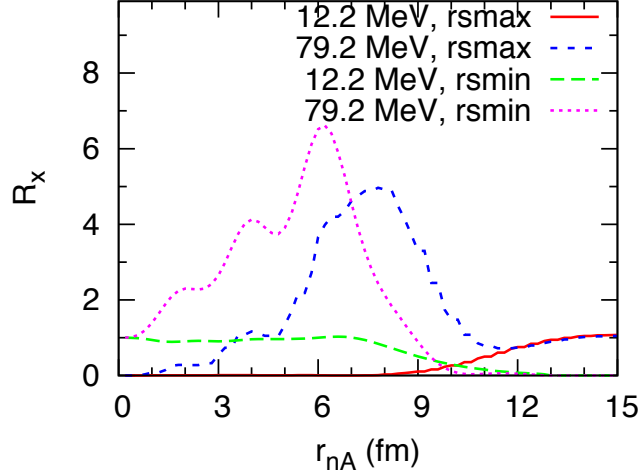


FIG. 22. (Color online) Dependence of the normalized ADWA differential cross sections R_x on r_{nA} for the deuteron stripping $^{116}\text{Sn}(d, p)^{117}\text{Sn}(3s_{1/2})$ at $E_d = 12.2$ and 79.2 MeV. Green dashed and magenta dotted line are R_x at 12.2 and 79.2 MeV, correspondingly. To get these R_x we calculated the post ADWA differential cross section at the peak of the angular distribution. The radial integral over r_{nA} is calculated for $r_{nA}^{min} \leq r_{nA} < \infty$. The calculated differential cross section is normalized to the full differential cross section. Similarly, solid red and blue short dashed lines are the post ADWA R_x calculated at 12.2 and 79.2 MeV, correspondingly, in which the radial integral over r_{nA} is calculated in the interval $0 \leq r_{nA} \leq r_{nA}^{max}$. Again the calculated differential cross sections are normalized to the full differential cross sections at the corresponding energies. Hence, r_{nA} on the abscissa is r_{nA}^{min} for the green dashed and magenta dotted lines and r_{nA}^{max} for the solid red and blue short dashed lines.

from the r_{nA}^{max} dependence of the R_x (solid red line). We can see the contribution to the reaction from $r_{nA} < 7.5$ fm can be neglected. Meantime at 79.2 MeV we observe quite a different behavior of R_x . The dependence on r_{nA}^{min} (magenta dotted line) shows that the internal region between 1 and 7.5 fm plays an important role what is drastically different from 12.2 MeV case.

Now we can apply the combined method to determine the SF from 79.2 MeV data using the ANC obtained from 12.2 MeV data. It can be done using Fig. 23 where we compare the absolute values of the ANCs from the ADWA calculations determined for the 12.2 and 79.2 MeV data. A sharp dependence on r_0 of the ANC obtained from the 79.2 MeV data confirms that the reaction is not peripheral. The high-energy ANC overlaps with the low-energy ANC

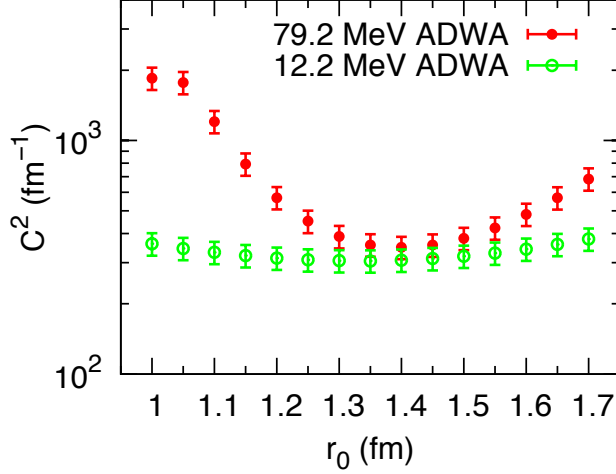


FIG. 23. (Color online) Comparison of r_0 -dependence of the ANCs in the ADWA for the deuteron stripping $^{116}\text{Sn}(d, p)^{117}\text{Sn}(3s_{1/2})$ at $E_d = 12.2$ MeV and 79.2 MeV. Green open dots show the r_0 -dependence of the ANC determined from 12.2 MeV reaction and red filled dots is the ANC from 79.2 MeV. For simplicity, in the ANC the subscripts denoting quantum numbers are omitted.

in the interval $1.35 \leq r_0 \leq 1.5$. It corresponds to the SF $0.14 \leq SF_{301/2} \leq 0.24$. Note that the existing data and their uncertainty does not allow us to determine the the SF with better accuracy.

The standard analysis of the 12.2 MeV data with the geometry $r_0 = 1.17$ fm and $a = 0.72$ fm in [18] gave $SF_{301/2} \geq 0.5$. Note that the optical potentials used in [18] are different from the CH89 optical potentials adopted here. If we use the bound-state potential geometry from [18] in the ADWA employed here (CH89 optical potentials and with non-locality corrections) we get even higher SF, $SF_{301/2} = 0.89$. The corresponding ANC is $C_{01/2}^2 = 667 \text{ fm}^{-1}$. If we use the standard geometry for the neutron bound-state potential, $r_0 = 1.25$ fm and $a = 0.65$ fm, from the ADWA analysis with CH89 optical potentials and non-locality effects from the 79.2 MeV data we get the SF $SF_{303/2} = 0.52$, which is close to the result from [18]. However, the corresponding ANC is $C_{01/2}^2 = 451 \text{ fm}^{-1}$ (red filled dots in Fig. 23). Thus higher SF can be obtained only on the expense of the ANC, which is significantly higher of the interval $C_{03/2}^2 = 310 \pm 30 \text{ fm}^{-1}$ determined from the low-energy data.

The r_0 interval, in which the ANC determined from 79.2 MeV data coincide with the ANC extracted from the 12.2 MeV data, is located at $r_0 > 1.25$ fm where the SF is lower than 0.5. As we see from Fig. 23 the ANC decreases with r_0 increase (until $r_0 \approx 1.4$ fm).

Such a behavior follows from Eq. (22) if we assume the destructive interference between the external and internal amplitudes with the dominance of the external part. Overestimation of the internal part leads to a smaller denominator in Eq. (22) and to a bigger extracted ANC at the standard geometry. Thus, as in the case of the deuteron stripping on ^{58}Ni , too high ANC at the standard geometry is caused by the overestimation of the internal part of the reaction amplitude. If we take, for example, $r_{nA}^{min} > 1$ fm, we see that the internal part decreases with increase of r_{nA} (the external part does not depend on $b_{301/2}$, that is, on r_0) leading to increase of the theoretical cross section and to decrease of the extracted ANC. Hence, the r_0 -dependence of the ANC calculated at 79.2 MeV intersects with the ANC curve at 12.2 MeV at large r_0 (or $b_{301/2}$), at which the SF becomes very small. If the internal contribution is smaller than in the CDCC theory, then the theoretical differential cross section is larger and the intersection of the higher energy ANC with the ANC curve at 12.2 MeV will occur at $r_0 < 1.35$ fm $^{-1}$, what leads to higher SF making the ANC and SF more compatible.

Thus, the low SF extracted using the combined method reveals one of the main shortcomings of the reaction theory - inadequate description of the internal region. This flaw was hidden in the standard approach, in which the geometry of the bound state potential could vary arbitrarily on the expense of the ANC to determine the SF.

V. SUMMARY

We have presented the analysis of three different deuteron stripping reactions, $^{14}\text{C}(d, p)^{15}\text{C}$, $^{58}\text{Ni}(d, p)^{59}\text{Ni}$ and $^{116}\text{Sn}(d, p)^{117}\text{Sn}$. Each of the reactions is analyzed at two different energies. At low energy all the reactions are peripheral and the experimental ANCs are determined with accuracy $\sim 10\%$. After that from the analysis of these reactions at significantly higher energies we determine the SF by fixing the normalization of the peripheral amplitude governed by the ANC found from the low-energy reactions. This two-step procedure constitutes the combined method of determination of the SF. The determined ANCs and SFs for all three cases are given in the cumulative Table V

In the combined method the problem of the extraction of the spectroscopic information from the deuteron stripping reaction is made on the clear physical basis: the ANC determines the normalization of the peripheral part of the reaction amplitude and determining the ANC

TABLE VII. ANCs $C_{l_{nA} j_{nA}}^2$ and spectroscopic factors $SF_{l_{nA} j_{nA}}$ from the $^{14}\text{C}(d, p)^{15}\text{C}$, $^{58}\text{Ni}(d, p)^{59}\text{Ni}$ and $^{116}\text{Sn}(d, p)^{117}\text{Sn}$ reactions.

Reaction	$C_{l_{nA} j_{nA}}^2 \text{ fm}^{-1}$	$SF_{l_{nA} j_{nA}}$
$^{14}\text{C}(d, p)^{15}\text{C}(2s_{1/2})$	1.80 ± 0.2	0.82 ± 0.03
$^{58}\text{Ni}(d, p)^{59}\text{Ni}(2p_{1/2})$	111.7 ± 12	≤ 0.19
$^{116}\text{Sn}(d, p)^{117}\text{Sn}(3s_{1/2})$	310 ± 30	$0.14 - 0.24$

we can fix the external part; the SF is mainly contributed by the internal part and it can be determined at the fixed external part. Hence the combined method imposes a strict limitation on the variation of the geometrical parameters of the Woods-Saxon potential, which can be arbitrarily taken in the standard approach. By checking compatibility of the ANC and SF the combined method tests also the accuracy of the contemporary reaction theory in treating the nuclear interior, which is the most crucial part in determination of the SF.

In the analysis three approaches, DWBA, ADWA and CDCC have been used. The application of the combined method allowed us to determine the ANC and SF for the reaction $^{14}\text{C}(d, p)^{15}\text{C}$ with loosely bound neutron. The analysis shows that the determined ANC and SF are compatible in this case. The success in this case is related with the fact that at higher energy the internal part of the reaction amplitude is contributed by the region close to the surface of the target ^{14}C while the deep internal region, where the theory may not be accurate, is suppressed.

However, we observe quite a different picture for the deuteron stripping reaction on heavier nuclei, ^{58}Ni and ^{116}Sn with high neutron binding energies. For higher energies the contribution from the nuclear interior becomes very important. The flaw in the treatment of the nuclear interior in the nuclear reaction theory, which is hidden in the standard approach, is immediately revealed as incompatibility of the ANCs and SFs. We demonstrate that the SFs determined in the previous publications using the standard method are done on the expense of the ANC, which becomes significantly higher than the experimental values. If we include the information about the experimental ANCs then the determined SFs become

too low. That is the meaning of the incompatibility of the ANC and SF in these cases. We conclude that to obtain a reliable spectroscopic information the improvement of the treatment of the internal region is necessary. The surface integral formalism and the generalized R -matrix method may be a possible solution [20, 21].

ACKNOWLEDGMENTS

DYP gratefully acknowledges the supports of the National Natural Science Foundation of China (Grant Nos. 11275018 and 11035001) and the Chinese Scholarship Council (Grant No. 201303070253). A.M.M. acknowledges that this material is based upon work supported by the U.S. Department of Energy, Office of Science, Office of Nuclear Science, under Award Numbers DE-FG02-93ER40773 and DE-SC0004958. It is also supported by the U.S. Department of Energy, National Nuclear Security Administration, under Award Number DE-FG52-09NA29467 and by the US National Science Foundation under Award PHY-1415656.

-
- [1] S. A. Goncharov et al., Sov. J. Nucl. Phys. **35**, 383 (1982).
- [2] A. M. Mukhamedzhanov and F. M. Nunes Phys. Rev. **C 72**, 017602 (2005).
- [3] D. Y. Pang, F. M. Nunes and A. M. Mukhamedzhanov, Phys. Rev. **C 75**, 024601 (2007).
- [4] A. M. Mukhamedzhanov, F. M. Nunes, and P. Mohr, Phys. Rev. **C 77**, 051601(R) (2008).
- [5] M. McCleskey *et al.*, Phys. Rev. **C 89**, 044605 (2014).
- [6] A. J. Koning and J. P. Delaroche, Nucl. Phys. **A713**, 231 (2003).
- [7] R. L. Varner, Physics Reports **201** (2), 57 (1991).
- [8] R. C. Johnson and P. C. Tandy, Nucl. Phys. **A235**, 56 (1974).
- [9] N. Austern, Y. Iseri, M. Kamimura, M. Kawai, G. Rawitscher, M. Yahiro, Phys. Rep. **154**, 125 (1987).
- [10] L. D. Blokhintsev, I. Borbely, and E. I. Dolinskii, Fiz. Elem. Chastits At. Yadra **8**, 1189 (1977) [Sov. J. Part. Nuclei **8**, 485 (1977)].
- [11] M. Kawai, M. Kamimura, and K. Takesako, Prog. Theor. Phys. Suppl. **89**, 118 (1986).
- [12] W. W. Daehnick, J. D. Childs, and Z. Vrcelj, Phys. Rev. **C 2 1**, 2253 (1980).
- [13] I. J. Thompson, Comput. Phys. Rep. **7**, 167 (1988).
- [14] J. A. Tostevin, University of Surrey version of the code TWOFNR of M. Toyama, M. Igarashi, and N. Kishida, <http://www.nucleartheory.net/NPG/code.htm> .
- [15] J. A. Aymar, H. R. Hiddleston, S. E. Darden and A. A. Rollefson, Nucl. Phys. **A207**, 596 (1973).
- [16] K. Hatanaka, *et al.*, Nucl. Phys. **A419**, 530 (1984).
- [17] O. Iwamoto *et al.*, Nucl. Phys. **A576**, 387 (1994).
- [18] C. Lapointe, J. Birchall, N. Videla *et al.*, Nucl. Phys. **A451**, 21 (1986).
- [19] V. R. Cupps, J. D. Brown, C. C. Foster *et al.*, Nucl. Phys. **A469**, 445 (1987).
- [20] A. M. Mukhamedzhanov, Phys. Rev. **C 84**, 044616 (2011).
- [21] A. M. Mukhamedzhanov, D. Y. Pang, C. A. Bertulani, and A. S. Kadyrov, Phys. Rev. **C 90**, 034604 (2014).